

LES study of the influence of the vortex generators on cooling of surface-mounted cubes

Hassan, Hemida; Siniša, Krajnović

Division of Fluid Dynamics, Department of Applied Mechanics, Chalmers University of Technology, SE-412 96 Gothenburg, SWEDEN

ABSTRACT

The influence of vortex generators on the enhancement of heat transfer from a wall-mounted cube matrix was investigated by numerical simulation using finite-volume method. The momentum and convective heat transfer equations were discretized and solved using large-eddy simulation. The numerical simulation was performed on a fully developed turbulent flow over one cube mounted in the middle of a cube matrix. Constant heat flux was generated from the cubes. Periodic boundary conditions were applied in both the streamwise and the spanwise directions. In order to study the influence of vortex generator on the flow structures and heat transfer coefficient, the flow and the convective heat transfer equations were solved around two cube configurations: a smooth cube and a cube with vortex generator attached to its surface. The vortex generator used in this investigation is a simple rib attached to the top and the side walls of the cube close to the streamwise edge. The flow Reynolds number based on the bulk velocity and the height of the channel was 13000. Standard Smagorinsky subgrid-scale model was used to model the unresolved scales and heat fluxes. The LES results were compared with the experimental results and good agreement was obtained. Numerical flow visualization was used to provide a better insight into the flow structures and heat transfer coefficient around the cubes. The LES results showed that the flow in the boundary layer around the cube with vortex generator is more turbulent and unsteady than the flow around the smooth cube without the vortex generator. More turbulent structures are generated close to the surface of the cube resulting in a good mixing of heat and hence high heat transfer coefficient.

1. INTRODUCTION

When electronic components are attached to a printed circuit, they, under concentrated heat dissipation condition, act as a strong source of heat which might cause local overheating. It is generally believed that local overheating of integrated circuits (IC) is the major cause for the technical failure of electronic equipment. Hence, finding a way for an efficient heat removal from these components is crucial to ensure steady reliable long-term operations. The production and development of new generation of power-electronic components is controlled by the efficient design to remove the heat

generated by these components. In general the heat removal from an integrated circuit depends very much on the flow structure around it. The electronic component is a bluff body that produces flow with separations. The flow around an integrated electronic circuit can be approximated to be similar to the flow around a cube mounted on a surface. Previous investigations of the flow around a surface-mounted cube found that different kinds of flow instabilities give rise to different flow structures around the cube. At low and moderate Reynolds numbers, the flow separates from the side of the cube to form separation bubbles. The flow inside these bubbles circulates and it might be rapped in its place if the bubbles are steady. The shear layers between these separation bubbles and the exterior fluid are highly turbulent and this gives rise to so-called the Kelvin-Helmholtz flow instability. This flow instability is responsible for shedding of vortex tubes in a regular fashion to the wake flow behind the cube, distortion of large scale vortices, production of small scales and eventually transition from laminar to turbulent flow. There is also flow instability in the wake flow behind the cube which is associated with the shedding of large scale vortices from the recirculation region to the far wake flow. This flow instability is controlled by the flow Reynolds number and hence the high frequency mode in the shear layers between the recirculation region and the exterior fluid. The dominated shear layers around the cube make the flow structures very complicated. Different numerical methods have been used in past to study the flow around a single cube mounted on a surface. Krajnović and Davidson [1] and [2] used large-eddy simulation to investigate the flow structures around a surface-mounted cube in a fully developed channel flow. They used different technique to visualize the flow. In their simulation, the Reynolds number was 40000 based on the incoming mean bulk velocity and the cube height. They found that the flow separates from the surface of the cube on the lateral and the top side faces of the cube. They visualized horse-shoe vortex attached to the mounting surface. Cone-like vortices are formed on the top-side face. These complex-flow structures are obtained using different flow simulations. The results were in a good agreement with the experimental results of Martinuzzi and Tropea [3]. Yakhot *et al.* [4] studied the same cube using Direct Numerical Simulation (DNS) and they got similar flow structures. . The

turbulent flow around a multiple cubes is even more complicated. The wake structures from one cube interact with the structures of the other cubes and the mounting surface. The flow is characterized by the complex interior topology which induces the flow to separate and recirculate locally between the mounting surface and the cubes. The shedding of the large scale structures in the wake flow depends mainly on the flow Reynolds number and on the separation distance between the cubes. The flow structures, however, are highly unsteady and three-dimensional. At present, there are remarkably few studies on local heat transfer around a three-dimensional object [5]. Meinders and Hanjalić [6] experimentally investigated the influence of the relative obstacle position on the convective heat transfer from a configuration of two wall-mounted cubes located in a fully developed turbulent channel. They found that the crucial parameter that influences the flow pattern and, consequently, the heat transfer is the longitudinal spacing between the cubes. Meinders and Hanjalić [7] investigated experimentally a matrix of equidistant cubes mounted on one of the walls of a plane channel. Their investigation provided reference data on flow and heat transfer relevant to electronics circuitry. The investigations were done on an internally heated cube that was placed in the middle of the matrix of identical but nonheated cubes; all mounted on a constant temperature channel wall (See [7] and [8]). The surrounding cubes on the matrix ensured a fully developed flow with periodic boundary conditions. Due to the well-known boundary condition and its computational simplicity, their case and data are considered the bases for many of computational fluid dynamic simulations to get insight into the physics of the flow structures and heat transfer. Cheng *et al.* [9] and Zhong and Tucker [10] used the experimental data of Meinders and Hanjalić [7] to compare different simulation techniques (large-eddy simulation (LES), standard κ - ϵ Reynolds-Averaged Navier-Stokes (RANS) and k - l based hybrid LES/RANS). Despite that many attempts have been done in the past to understand the physics of the flow around single or multiple cubes very few attempts were performed to find a way to enhance the heat transfer from the cubes. In this paper, we investigate the influence of altering the turbulent boundary layer on the surfaces of the cubes on the enhancement of heat transfer. This is done by generating small vortices on the surface of the cube using vortex generator. The vortex generator in the present work is a simple rib mounted on the top and the side faces of the cubes. The Reynolds number of the flow is 13000, based on the incoming bulk velocity and height of the cube. The objective of the present work is to employ LES to investigate the influence of the vortex generators on the flow structures and the local heat transfer coefficient.

2. PHYSICAL MODEL

The physical model was a single heated cube placed in the middle of an equidistant matrix of surface-mounted cubes as shown in Fig.1. The matrix of cubes was placed on one of the walls of a two-dimensional channel. The matrix consisted of a total of 25x10 cubes in the

streamwise and spanwise directions, respectively. The side length of the cubes, H , was 15 mm. The height of the channel was 51 mm ($3.4H$). The distances between the centerlines of the cubes in the streamwise and the spanwise directions were 60 mm ($4H$).

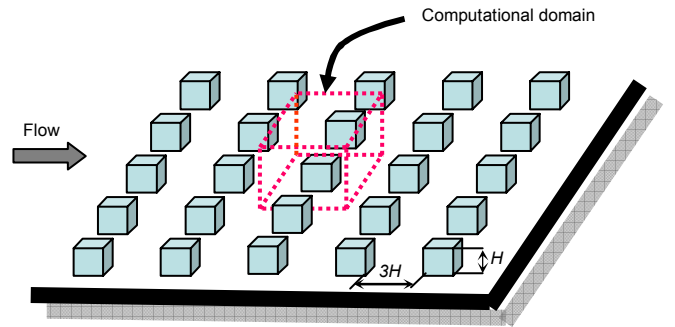


Figure 1. Matrix of cubes mounted on a wall.

3. GOVERNING EQUATIONS

Since the flow is unsteady an unsteady numerical method for the prediction of the flow and heat transfer is needed. The Direct Numerical Simulation (DNS) is computationally demanding due to the very large number of nodes needed to resolve all the large as well as the dissipative scales. The flow around a cube is a typical bluff body flow where the flow is dominated by large separation and recirculation regions. Previous investigation of the flow around bluff bodies showed that Reynolds-Averaged Navier-Stokes (RANS) methods give poor results compared to Large-Eddy Simulations (LES). In this paper, the LES was employed to solve for both the velocity and temperature fields. In LES, the large eddies are computed directly and the influence of the small-scale eddies on the large-scale eddies are modeled. The incompressible continuity, momentum and heat equations are filtered using an implicit spatial filter. The resulting filtered equations are:

$$\frac{\partial \bar{u}_i}{\partial x_i} = 0 \quad (1)$$

$$\frac{\partial \bar{u}_i}{\partial t} + \frac{\partial}{\partial x_j} (\bar{u}_i \bar{u}_j) = -\frac{1}{\rho} \frac{\partial \bar{p}}{\partial x_i} + \nu \frac{\partial^2 \bar{u}_i}{\partial x_j \partial x_j} - \frac{\partial \tau_{ij}}{\partial x_j} \quad (2)$$

and

$$\frac{\partial \bar{T}}{\partial t} + \frac{\partial}{\partial x_j} (\bar{u}_j \bar{T}) = \frac{\nu}{Pr} \frac{\partial^2 \bar{T}}{\partial x_j \partial x_j} - \frac{\partial h_j}{\partial x_j} \quad (3)$$

Here, \bar{u}_i , \bar{p} and \bar{T} are the resolved filtered velocity, pressure and temperature, respectively. Owing to the non-linear terms in the momentum and heat equations, the filtered-out small scale eddies feed back their effects on the large-scale motion through subgrid-scale stresses and heat fluxes. These influences appeared as extra terms in the filtered equations, i.e. τ_{ij} and h_j . The subgrid scale (SGS) stresses $\tau_{ij} = \overline{u_i u_j} - \bar{u}_i \bar{u}_j$ represent the influence of the unresolved scales, smaller than the filter

size, on the resolved ones. The subgrid-heat fluxes, $h_j = \overline{u_j T} - \overline{u_j} \overline{T}$, represent the influence of the unresolved heat fluxes on the resolved ones. These subgrid stresses and heat fluxes are unknowns and must be modeled. The standard Smagorinsky model was used in the present work to model the SGS stresses and the heat fluxes. This model was used due to its simplicity and in order to reduce the computational cost. The origin of this model is based on the assumption of the equilibrium between the production and dissipation for the small scales. In this model, the subgrid-scale stresses and heat fluxes are modeled as:

$$\tau_{ij} - \frac{1}{3} \delta_{ij} \tau_{kk} = -2\nu_{sgs} \overline{S}_{ij} \quad (3)$$

and

$$h_j = -\alpha_t \frac{\partial \overline{T}}{\partial x_j}, \quad (4)$$

where ν_{sgs} is the subgrid-scale viscosity, α_t is the subgrid-scale eddy diffusivity and \overline{S}_{ij} is the resolved rate of strain tensor defined as:

$$\overline{S}_{ij} = \frac{1}{2} \left(\frac{\partial \overline{u}_i}{\partial x_j} + \frac{\partial \overline{u}_j}{\partial x_i} \right). \quad (5)$$

The subgrid-scale viscosity, ν_{sgs} , is defined as:

$$\nu_{sgs} = (C_s \Delta)^2 |\overline{S}| \quad (6)$$

where the magnitude of the local strain rate tensor is defined by $|\overline{S}| = \sqrt{2\overline{S}_{ij}\overline{S}_{ij}}$, Δ is the filter width taken as the cubic root of the volume of the finite volume cell and C_s is the model constant. The value of the model constant in the present work was 0.1. Similar to the subgrid-scale viscosity, the subgrid scale eddy diffusivity, α_t , is defined as:

$$\alpha_t = \frac{1}{Pr_t} (C_s \Delta)^2 |\overline{S}| \quad (7)$$

where Pr_t is the subgrid-scale Prandtl number. The value of Pr_t was taken as 0.6 in this paper. The Smagorinsky model is widely used in the simulations of bluff body flow (see [10], [11] and [12]). It used also in modeling of the unresolved fluxes in the simulations of heat transfer problems (see [13]).

4. COMPUTATIONAL DOMAIN AND BOUNDARY CONDITIONS

The size of the computational domain was $4H \times 3.4H \times 4H$ as shown in Fig. 2. Similar to the experimental setup of Meinders and Hanjalić [6], the test cube was chosen to be in the middle of the cube matrix where the flow is fully developed in both the streamwise and the spanwise directions. Due to the periodicity of the flow around the cubes, periodic boundary conditions were applied in the streamwise and the spanwise directions for the velocity field. No-slip boundary conditions were employed at solid walls.

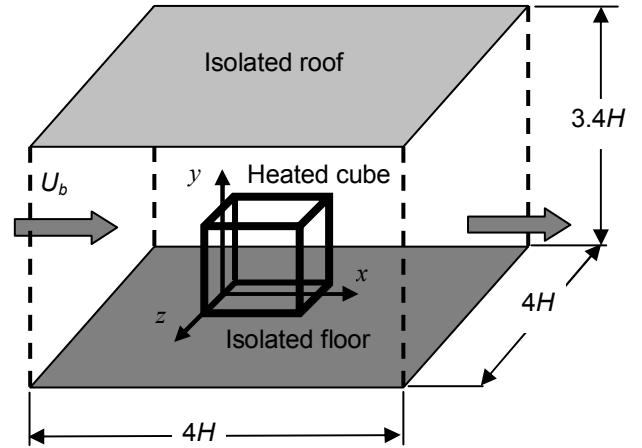


Figure 2. The computational domain

The x and y axes were taken in the streamwise and wall-normal directions, respectively while the z direction denoted the spanwise direction. The coordinate system originates from the channel wall at the center of the windward face of the cube, as shown in Fig. 2. The bulk velocity of the incoming flow was 3.86 m/s yielding the value of the Reynolds number of 13000, based on the incoming bulk velocity and the height of the channel. The density of the air was 1.16 kg/m^3 and its dynamic viscosity was $1.5 \times 10^{-5} \text{ m}^2/\text{s}$. A constant mass flow rate of 0.0137 kg/s was passed from the sub channel. The value of the Prandtl number of the air was 0.71.

The rate of heat dissipated from an individual cube to the air was constant and equal to 2 Watt. This made the temperature rise between any two successive cubes to be constant. Periodic boundary conditions for the temperature and temperature rise were applied in the spanwise and streamwise directions, respectively. The bulk temperature for the incoming flow was $294 \text{ }^\circ\text{K}$. The channel walls were insulated. The commercial finite volume solver, Fluent 6.2, was employed to solve the filtered equations. The convective and viscous diffusion plus the subgrid-scale fluxes were approximated by second order-accurate central difference scheme. were used in the simulations. The time integration was done using the Crank-Nicolson second-order scheme.

5. VORTEX GENERATORS

The vortex generators (VGs) are small devices primarily used to suppress the formation of the separation regions and to alter the aerodynamic coefficients by changing the flow structures around the bodies. As an example, VGs are used on the wing of airplanes to prevent separations and hence increase the lift coefficient. They are used inside gas turbines to reduce the pressure drop due to flow separation. The influence of the flow separation is always negative for the aerodynamic coefficient and pressure drop. In case of heat transfer, flow separation might enhance or discard the heat transfer. The points where the flow separates and reattaches to the body are always associated with local increase of heat transfer coefficient due to the high turbulent intensity in the shear layers close to these

points. On the other hand, the flow trapped in the separation region and recirculation regions undergoes local heating, reducing the heat transfer coefficient.

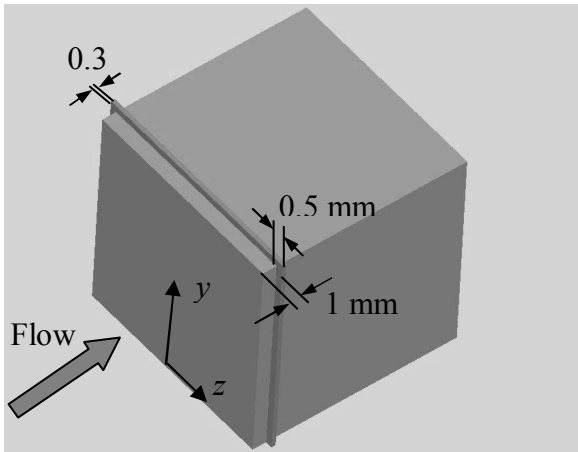


Figure 3. The shape of the vortex generator.

In order to enhance the heat transfer from the surface of the cubes, it is highly desired that the boundary layers on the surface of the cubes are turbulent. The turbulent boundary layer implies high local mixing due to the small scale vortices and hence high convective heat transfer coefficient. One way to attain a turbulent boundary layer on the surface of the cubes is to use vortex generators (VGs). These VGs are very small devices attached to the surface of the cube in the places where boundary-layer separation is expected. Another advantage of the VGs is the formation of large scale vortices behind them. The shape of the VGs determines by high extend the shape of these vortices. These vortices are highly unsteady and they shed from the recirculation region behind the VGs at a regular frequency (the shedding frequency of the wake behind the VGs). The size of these vortices is of the order of magnitude of the size of the VGs which is of the order of magnitude of the height of the boundary layer thickness without the VGs. That means that the new boundary layer on the surface of the cube with VGs is dominated with vortices that are more turbulent, unsteady and larger in scale than those in the boundary layer without VGs. These new large structures on the surface of the cube help carrying the heat from the surface and viscous sublayer to the exterior fluid and hence increase the heat transfer coefficient. The shape of the VG used in this work is shown in Fig. 3. It is a simple rib attached to the side and top faces of the cube at a distance 1 mm from the windward edge of the cube. This position is corresponding to the start position of the separation on the side and top face of the cube in case if the VG is not attached. The thickness of the VG is 0.3 mm and its height is 0.5 mm.

6. COMPUTATIONAL GRID

Unstructured computational grids, consist of *O* and *C* topology, were used in both of the simulations around the smooth cube without VG and around the cube with VG. The shapes of these grids for the cube without and with the VG are shown in Figs 4 and 5, respectively.

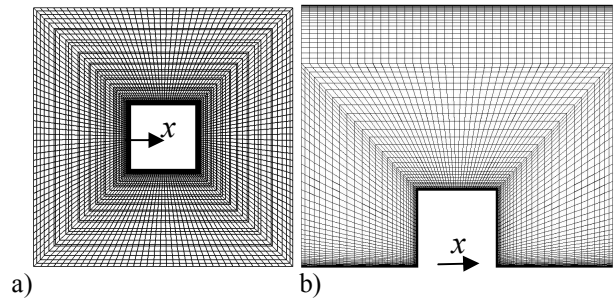


Figure 4. Grid topology around cube without VG.

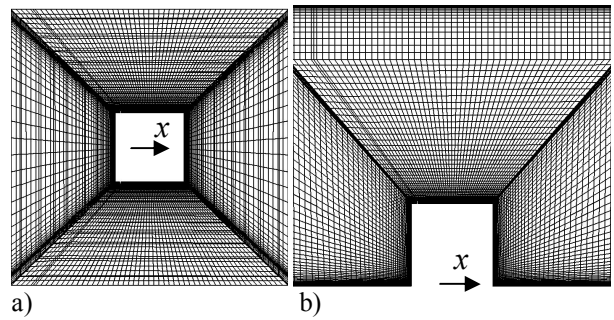


Figure 5. Grid topology around cube with VG.

The total number of nodes was 400,000 for the simulation over the cube without VG. Fifteen nodes, covered the height of the VG, were used to resolve the flow in the wake of the VG. As a result, the computational grid for the case with VG increased to 900,000 nodes. The centers of all the boundary cells have a distance of 0.009 mm (0.004 H) to the wall. This distance ensured that $y^+ < 1$ for the first row of cells next to the wall. Since second-order accurate central difference scheme was used in the discretization of both convective and diffusive terms, which is sensitive to the grid stretching, the stretching ratio of the grid did not exceed 1.1 for any two successive nodes.

7. RESULTS

In this section, the influence of the VG on the time-averaged flow, the instantaneous flow and the heat transfer coefficient is explained. The simulation was performed using a constant time step of 0.00015 yielding a maximum CFL number of less than 1.0. The simulation started with a uniform streamwise velocity equal to the bulk velocity. The other two components of the velocity are set to zero value. The momentum equation was solved first while the energy equation is turned off. After the solution was converged and a fully developed flow was obtained, the energy equation was activated while the velocity field was frozen. When converged solution was obtained for the temperature field, the averaged process started. The time-averaged data were obtained using 20,000 time steps. Meinders and Hanjalić [6] found that the shedding frequency was corresponding to a Strouhal number of $St=0.109$ based on the height of the cube and the incoming bulk velocity. This means that the time-averaged data were gathered over 15 shedding cycles. Figure 6 shows the streamwise velocity distribution on the vertical xy -plane at $z/H=0$ at five different locations in the streamwise direction ($x/H=-0.3, 0.5, 1.3, 1.5, 2$). The figure shows good

agreement between the LES data and the experimental data of Meinders [6] meaning that the mesh resolution is fine enough to resolve the flow and hence the heat transfer. Figure 7 displays the time-averaged flow structures around the smooth cube by means of streamlines projected to xy -plane and xz -plane at $z/H=0$ and $y/H=0.006$, respectively. The flow impinges on the streamwise face of the cube causing stagnation region with high pressure. The stagnation line was noticed in Fig.7.a at $y/H \approx 0.8$. Due to the high pressure in the streamwise face, the flow moves up, down and towards the lateral faces. The part of the flow that moves downward is forced to change its direction again due to the second stagnation region on the mounting surface. This makes it circulate around the cube forming the horse-shoe like vortex. The part of the flow that moves toward the top and lateral faces separates from the surfaces of the cube before it reattaches again to the surface. Separation bubbles are shown in Fig.7.a and 7.b.

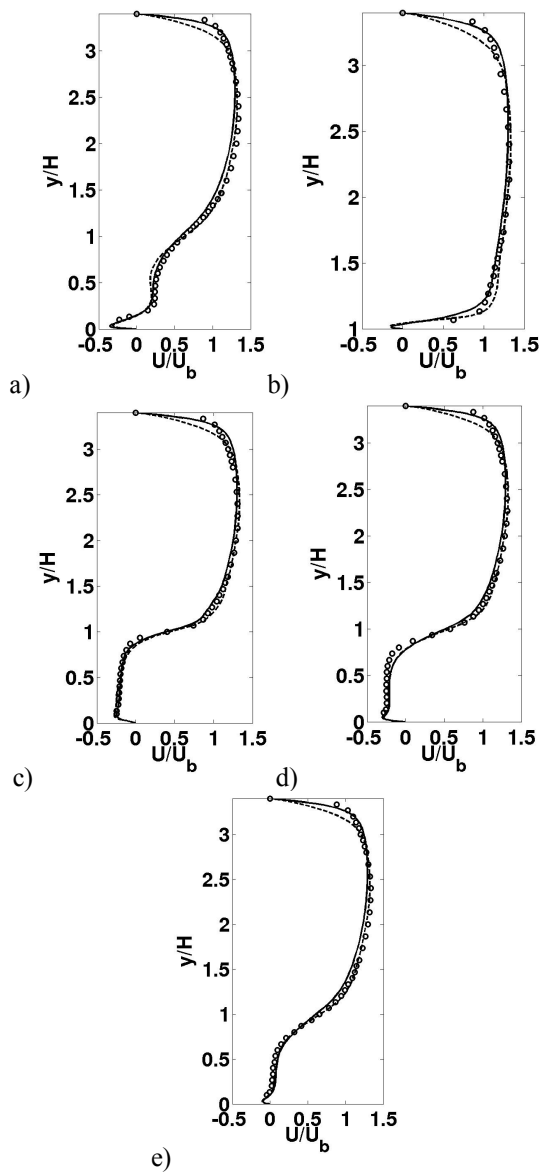


Figure 6. Streamwise velocity profile in vertical xy -planes at $z/H=0$ and a) $x/H=-0.3$, b) $x/H=0.5$, c) $x/H=1.3$, d) $x/H=1.5$, e) $x/H=2$. Symbols: experimental results (Meinders [6]); solid lines: LES (smooth cube); dashed: LES (cube with VG).

Figure 7.a shows a clear circulation bubble in the wake next to the top face of the cube. The axis of this bubble is parallel to the spanwise direction (z -axis). Figure 7.b shows two recirculation regions in the wake of the cube. The coming flow from the sides of the cube separates from the surface and circulates on those recirculation bubbles. The axes of these recirculation bubbles are parallel to the normal direction of the mounting surface (y -axis). These two vortices are connected together through the upper-side vortex to form an arch-shape vortex behind the cube. Figure 8 shows the different time-averaged flow structure around the smooth cube. Figure 9 shows the time-averaged streamlines projected to the vertical xy -plane at $z/H=0$ and the xz -plane at $y/H=0.006$ in case of cube with VG.

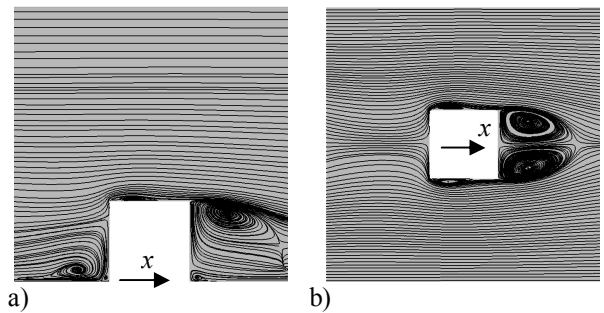


Figure 7. Cube without VG. Time-averaged streamlines of the flow around the cube in (a) the x/y -plane at $z/H=0$ and in (b) the xz -plane at $y/H=0.5$.

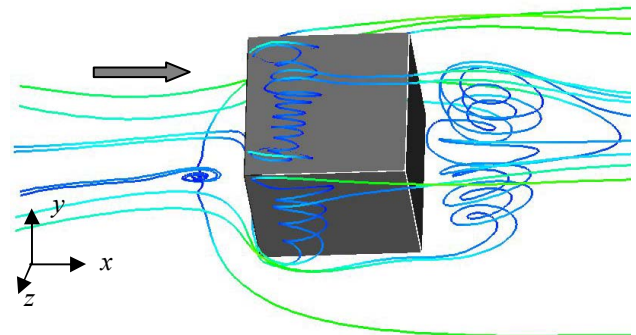


Figure 8. Flow structures around a cube without VG.

The time-averaged flow structures around the cube with VG are similar to that around the smooth cube without VG. The only difference between Fig.7 and Fig.9 is the size of the separation bubble on the top and the lateral side faces.

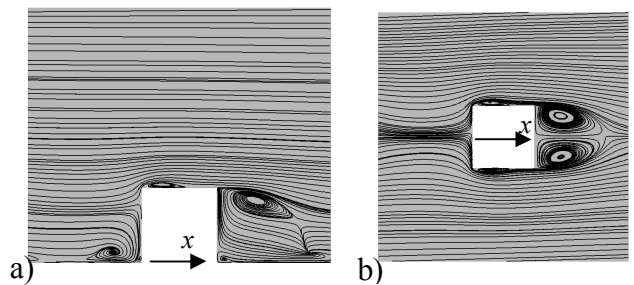


Figure 9. Cube with VG. Time-averaged streamlines of the flow around the cube in (a) the x/y -plane at $z/H=0$ and in (b) the xz -plane at $y/H=0.5$.

Although there are separation bubbles in the time-averaged flow on the sides of the cubes with and without VGs, the temporal evolution of these bubbles is completely different. In case of smooth cube without VG, the flow separates from the faces due to the adverse pressure gradient on the surface of the cube. On the other side, the bubbles that appear in the time-averaged flow on the top and side-faces of the cube with VG is mainly a result of the VG. Instantaneous pictures of the recirculation region behind the VG and of the separation region in case of cube without VG show that they behave in different ways. In case of smooth cube, the separation regions are almost stationary. The size of the separation bubbles is changing with regular frequency which is equal to the flow shedding frequency behind the cube. In case of recirculation region behind the VG, the boundary layer is characterized by relatively large-scale vortices. The vortices are shed from the recirculation region behind the VG to the boundary layer of the cube. The size of these vortices is of the order of magnitude of the size of the VG. The shedding frequency of these vortices is much higher than the dominant shedding frequency of flow behind the cube.

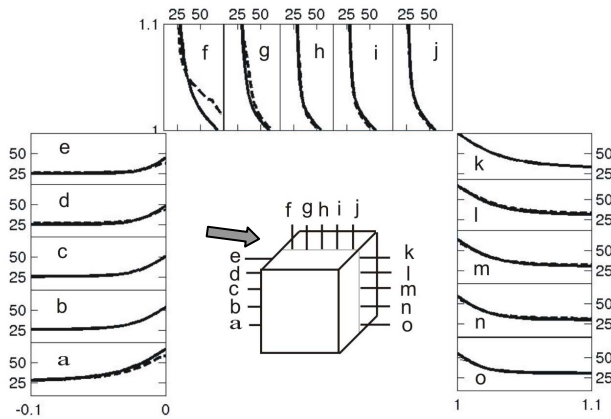


Figure 10. Temperature boundary layer profile in the vertical xy -plane at $z/H=0$. Here $y_a/H=y_o/H=0.1$, $y_b/H=y_n/H=0.3$, $y_c/H=y_m/H=0.5$, $y_d/H=y_l/H=0.7$, $y_e/H=y_k/H=0.9$, $x_f/H=0.1$, $x_g/H=0.3$, $x_h/H=0.5$, $x_i/H=0.7$, $x_j/H=0.9$. Solid line (LES over smooth cube); dashed line (LES over cube with VG)

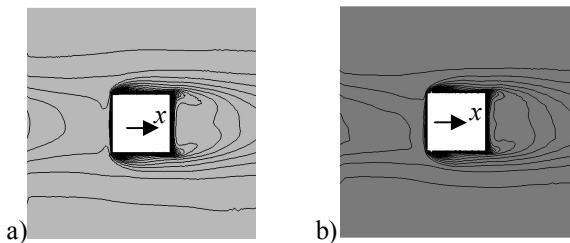


Figure 11. Contours of the time-averaged temperature distribution on xz -plane at $y/H=0.5$. (a) Cube without VG and (b) cube with VG.

Figure 10 shows the time-averaged temperature boundary layer profiles around the cubes at the vertical xy -plane at $z/H=0$. High temperature is reported on the surface of the cube in the places where flow separates or circulates. The time-averaged temperature distribution on the surface of the cube with VG is globally lower

than that on the surface of the cube without VG. Higher temperature spots are presented behind the VG (see Fig.10.f) where the heat is trapped inside the circulated flow in this region.

The shedding of vortices from the VG alters the wake structures behind the cube and hence the temperature distribution. This is shown in Fig.11 where a sharper temperature gradient is noticed in the wake of the smooth cube than that of the cube with VG. This observation is shown also in Fig. 10 as a reduction in the temperature of the streamwise and lee-side faces of the cube with VG. The temperature of the surface of the cube and the inlet bulk temperature are used to calculate the local heat transfer coefficient h as:

$$h = \frac{\dot{q}}{(T_s - T_b)} \quad (8)$$

Here \dot{q} is the heat flux, T_s is the surface temperature and T_b is the inlet bulk temperature. This definition makes the heat transfer coefficient a direct measure for the surface temperature which is suitable for judging the performance of the VG since the main goal is the cooling of the surface. To find out the influence of the flow structures on the heat transfer, the flow pattern on the surface of the cube with VG together with the corresponding local heat transfer coefficient h is shown in Fig. 12. Similarly, Fig. 13 shows the flow pattern on the surface of the smooth cube and the corresponding local heat transfer coefficient.

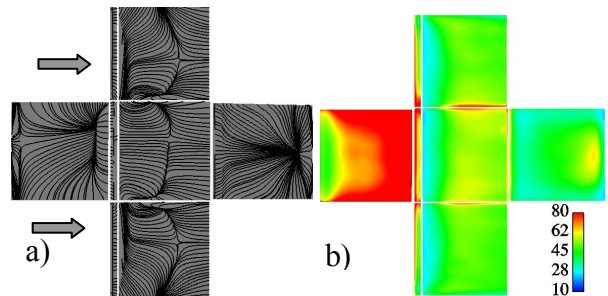


Figure 12. Cube with VG. (a) Time-averaged streamlines projected on a surface parallel to the five faces of the cube with a normal distance $0.0001H$ and (b) the corresponding map of the local heat transfer coefficient h (W/m^2K).

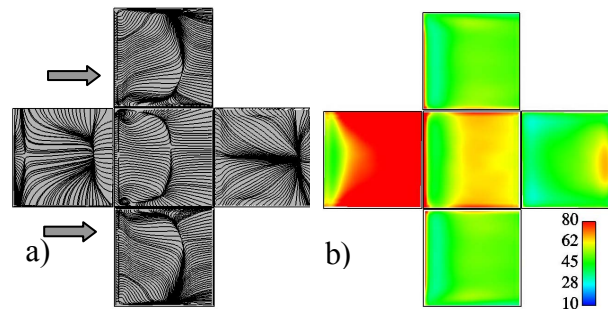


Figure 13. Cube without VG. (a) Time-averaged streamlines projected on a surface parallel to the five faces of the cube with a normal distance $0.0001H$ and (b) the corresponding map of the local heat transfer coefficient h (W/m^2K).

As expected, the temperature of the surface is high in the places associated with a flow separation. This is shown as low heat transfer coefficient on the side and top-side faces close to the leading edge and on the lee-side face next to the arch-like vortex. On the streamwise face, the downwash flow due to the stagnation region on the streamwise face carries the heat from the surface resulting in a high heat transfer coefficient. The interaction between the flow structure and the heat transfer is shown further in Fig. 14 by means of quantitative representations of the heat transfer coefficient at three different cross sections of the cube.

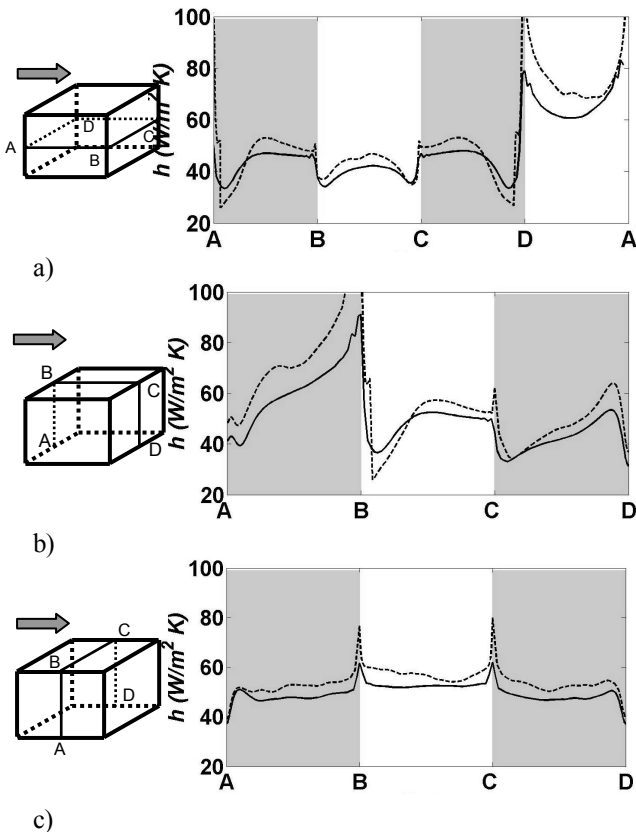


Figure 14. Distribution of the time-averaged local heat transfer coefficient along; a) the path ABCDA in the horizontal xz -plane at $y/H=0.5$, b) the path ABCD in the vertical xy -plane at $z/H=0$ and c) the path ABCD in the vertical yz -plane at $x/H=0.5$. Solid line (LES over smooth cube); dashed line (LES over cube with VG)

The mean time-averaged heat transfer coefficient obtained by the surface integrated heat flux and surface temperature is given in Table 1.

Although there are local high temperature spots behind the VG which are associated with decrease in local heat transfer coefficient, the global mean heat transfer coefficient is higher than the mean heat transfer coefficient of the cube without VG on all the faces of the cube. Table 1 shows that the front and the lateral-side faces have large enhancement of the mean heat transfer coefficient. There is an increase of the mean heat transfer coefficient of 25% on the front face while 9% increase is found on the lateral-side faces. The minimum enhancement of the heat transfer coefficient is

found on the top-side face (6.5 % increases). Globally, there is enhancement of the heat transfer coefficient of about 13.7% when VG is used.

Table 1. Mean heat transfer coefficient at each face of the cube.

Cube face	Cube without VG	Cube with VG	Percentage increase
Front	65.96	82.87	25.64
Top	49.75	52.93	6.39
Lee-side	38.79	44.19	13.92
Lateral-sides	45.05	49.06	8.90
Cube average	48.92	55.62	13.70

8. CONCLUSIONS

Large-eddy simulation was successfully used to investigate the influence of a rib-shape vortex generator, on the surface of a wall-mounted heated cube, on the local heat transfer coefficient. A topology consisting of *C* and *O* grids was used in the simulations which reduced, considerably, the number of cells needed for good spatial resolution. LES results for flow and temperature distribution were obtained for a surface-mounted cube with and without vortex generator. LES results were found to be in a good agreement with the experimental data for the case without VG for which the experimental data exist.

The relation between the flow structure around the cube and the temperature distribution is explained in the paper. The streamwise face of the cube was found to have high heat transfer coefficient due to the downwash flow that, efficiently, carries the heat from the face. Lower local heat transfer coefficient is reported on the places where flow separation occurs such as on the top-side face and the lee-side face of the cube close to the arch-shaped vortex.

It was found that the VG on the top and lateral faces of the cube altered the boundary layer on the surface of the cube. As a result, vortices are shed from the wake of the VG at a frequency higher than the dominant vortex shedding in the flow. These vortices are characterized by larger scale and large shedding frequency than the frequency of the boundary layer vortices without the VG. Globally these vortices enhanced mixing of heat in the boundary layer which appeared as high mean heat-transfer coefficient. The present investigation showed that the percentage increase of the heat-transfer coefficient is considerable on the front and lateral-side faces of the cube. Local high temperature spots are found in the circulation region behind the VG. There was an increase of the mean heat-transfer coefficient of about 25% in the front face while 9% increase was found in the lateral-side faces. The minimum

enhancement was found on the top-side faces (about 6.5 % increase). Globally, there was an enhancement of the heat-transfer coefficient of about 13.7% due to the attachment of the vortex generator on the surface of the cube.

9. REFERENCES

- [1] S. Krajnović, L. Davidson. "Flow Around a Three-Dimensional Bluff Body", *9th International Symposium on Flow Visualization*, Heriot-Watt University, Edinburgh, G.M. Carlomagno and I. Grant (Eds.), 2000.
- [2] S. Krajnović, L. Davidson. "Large-Eddy Simulation of the Flow Around a Bluff Body", *AIAA Journal*, Vol. 40(5), pp. 927-936, 2002.
- [3] R. Martinuzzi and C. Tropea. "The flow around surface-mounted prismatic obstacles placed in a fully developed channel flow" *ASME: Journal of fluids Engineering*, Vol., 115, pp. 85-91, 1993.
- [4] A. Yakhot, H. Liu, and N. Nikitin, "Turbulent flow around a wall-mounted cube: A direct numerical simulation", *International Journal of Heat and Fluid Flow* (in press), 2006.
- [5] H. Nakamura, T. Igarashi and T. Tusutsui, "Local heat transfer around a wall-mounted cube at 45° to flow in a turbulent boundary layer", *International Journal of Heat and Fluid Flow*, Vol., 24 (2003), pp. 807-815.
- [6] E. Meinders, and K. Hanjalić, "Experimental study of heat transfer from in-line and staggered configurations of two wall-mounted cubes", *International Journal of Heat and mass transfer*, Vol., 45 (3) (2002), pp. 465-482.
- [7] E. Meinders, and K. Hanjalić, "Vortex structure and heat transfer in turbulent flow over a wall-mounted matrix of cubes", *International Journal of Heat and fluid flow*, Vol., 20 (1999), pp. 255-267.
- [8] B. Ničeno, A. Dronkers and K. Hanjalić, "Turbulent heat transfer from a multi-layered wall-mounted cube matrix: a large eddy simulation", *International Journal of Heat and fluid flow*, Vol., 23 (2002), pp. 173-185.
- [9] Y. Cheng, F. Lien, E. Yee and R. Sinclair "A comparison of large-eddy simulations with a standard $\square\square$ Reynolds-averaged Navier-Stokes model for the prediction of a fully developed turbulent flow over a matrix of cubes", *Journal of Wind Engineering and Industrial Aerodynamics*, Vol., 91 (2003), pp. 1301-1328.
- [10] H. Hemida, S. Krajnović and L. Davidson, "Large-Eddy Simulations of the Flow Around a Simplified High Speed Train Under the Influence of a Cross-Wind", *17th AIAA Computational Fluid Dynamics Conference*, Toronto, Ontario, Canada 6-9 June, 2005.
- [11] H. Hemida, "Large-Eddy Simulation of the Flow around Simplified High-Speed Trains under Side Wind Conditions", thesis of Lic. of Engng, Division of Fluid Dynamics, Dept. of Applied Mechanics, Chalmers University of Technology, Göteborg, Sweden, 2006.
- [12] S. Krajnović, L. Davidson. "Flow Around a Simplified car, Part (1): Large-Eddy Simulation", *Journal of Fluid Engineering*, Vol. 127 (2005), pp. 907-918
- [13] D. Barhaghi and L. Davidson and R. Karlsson "Large Eddy Simulation of Natural Convection Boundary Layer on a Vertical Cylinder", Selected paper, *International Journal of Heat and Fluid Flow*, to appear, 2006.